A New Hybrid Multibias Analytical/Decomposition-Based FET Parameter Extraction Algorithm With Intelligent Bias Point Selection

Cornell van Niekerk, *Member, IEEE*, Johan A. du Preez, *Member, IEEE*, and Dominique M. M.-P. Schreurs, *Senior Member, IEEE*

***Abstract*—A new hybrid multibias analytical/decomposition-based parameter extraction procedure for GaAs FETs is described. The analytical calculations are integrated into an existing decomposition-based optimizer in a complementary approach, further increasing the robustness of the existing algorithm. It is illustrated that, in order to increase the reliability with which the full 15-element small-signal model can be extracted, it is necessary to exploit the underlaying characteristics of the system and the measured data used. This is achieved through the use of cold S-parameter data, along with simple modifications to the extraction algorithm, and a new intelligent selection algorithm for the active bias points used in the multi-bias extraction. The selection algorithm employs a simple geometric abstraction for the S-parameter data that allows it to select bias points that maximize the information available to the extraction procedure. The new selection algorithm shows for the first time what the influence of the bias points is on the performance of a multibias extraction procedure. Experimental results proving the robustness and accuracy of the described procedures are presented.**

***Index Terms*—Centroids, FET, modeling, multibias parameter extraction, S-parameters, selection algorithms, small-signal.**

I. Introduction

THE ability to generate measurement-based GaAs FET device models that are accurate enough to allow first-time design success for a variety of systems has long been a major goal of device modeling orientated computer-aided design (CAD) algorithms. The extraction of the small-signal model shown in Fig. 1 plays a crucial role in the construction of a large number of the nonlinear models that have been created to satisfy this goal.

The basic approach is to extract the small-signal model at a variety of different bias points and then use the variation of the intrinsic elements with bias to construct the nonlinear model. Such an experimental modeling approach requires that a large number of S-parameter measurements be processed, creating the need for extraction algorithms that can robustly perform large extractions without requiring user intervention or supervision. However, this requirement is made difficult by the ill-conditioned nature of the small-signal extraction problem. This causes both direct [1] and optimizer-based extraction procedures that process the data measured at different bias points separately to have difficulty in providing consistent solutions for all the elements in the small-signal model [2]. Several optimizer driven multibias extraction procedures [3]–[5] that combine data measured at different bias points into one unified problem have been proposed. These methods all assume that the extrinsic elements of the model in Fig. 1 are bias-independent. By combining data from different sources in the extraction algorithm, more information becomes available for determining a more unique solution.

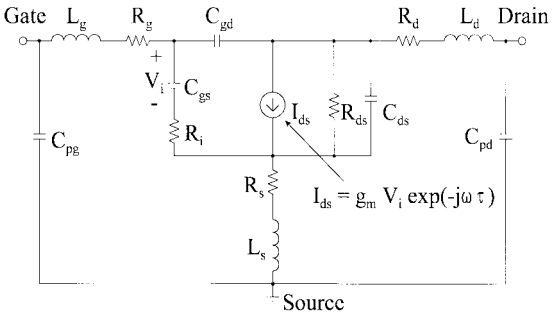

Fig. 1. 15-element small-signal model of a GaAs FET.

In [3] a multibias parameter extraction algorithm that exploits a decomposition-based optimization algorithm was presented. The procedure uses multiple sets of S-parameters measured at bias points in the active region of the device's $I_{\rm DS}$-$V_{\rm DS}$ plane and has been successfully applied to the modeling of both GaAs high electron-mobility transistor (HEMT) and MESFET devices. Active bias points at which the device is behaving as a nonreciprocal two-port provide the maximum amount of measured information per bias point. The extraction algorithm is built around an adaptive decomposition-based optimizer. This optimization procedure is independent of initial values and well suited to the ill-conditioned nature of the extraction problem. The decomposition approach can also efficiently handle large dimensional problems and is not as susceptible to the curse of dimensionality, as in more traditional optimization approaches.

Manuscript received March 26, 2002.

C. van Niekerk and J. A. du Preez are with the Department of Electrical and Electronic Engineering, University of Stellenbosch, Stellenbosch 7602, South Africa.

D. M. M.-P. Schreurs is with the ESAT-TELEMIC, Department of Electronic Engineering, Catholic University of Leuven, Leuven, Belgium.

Digital Object Identifier 10.1109/TMTT.2003.808631

In [3] a 13-element small-signal model which neglects the effect of $C_{\rm pg}$ and $C_{\rm pd}$ was extracted. The inclusion of the parasitic capacitors when dealing with on-wafer measured devices greatly increases the complexity of the problem. In practice, an extraction algorithm has to deal with several phenomena that make it difficult to achieve consistent results when extracting the full 15-element model shown in Fig. 1. One of the problems encountered is that the parasitic resistors R_d and R_s do not always adhere to the assumption of bias independence for the extrinsic elements. It has been found from experience that the value of R_d can appear to have a large bias dependence and assume values and a variation with bias that does not correspond to the physical reality. This in turn can make the determination of the other less dominant elements difficult. Another difficulty is the small size of the parasitic inductors L_g, L_d, and L_s of on-wafer measured devices. The small series impedance resulting from the parasitic inductors and resistors that separate $C_{\rm pg}$ and $C_{\rm pd}$ from the larger intrinsic capacitors makes it difficult to accurately extract the individual capacitor values. In many instances, device modelers are forced to absorb the effect of these two elements into the intrinsic capacitors by neglecting them from the small-signal model. $C_{\rm pd}$ can be especially difficult to determine, even for direct extraction algorithms that rely heavily on model simplifications. The difficulty in determining $C_{\rm pd}$ can also be seen in the variation of the extracted values of L_d, which exhibits strong interactions with $C_{\rm pd}$ [6], [7]. Since most of the model elements have complex interactions with each other, it should be noted that these potential problems should not be viewed in isolation from each other. Also, not all devices will exhibit all of the above-mentioned modeling difficulties.

This paper presents three extensions to the decomposition-based multibias extraction algorithm discussed in [3] which are able to overcome the discussed extraction difficulties.

In Section II, a new hybrid optimizer/analytical procedure aimed at improving the robustness and speed of the original procedure is presented. Analytical equations for the calculation of the intrinsic elements are integrated into the existing extraction procedure. Unlike other published algorithms [4], [5], [8], the analytical calculations do not replace any section of the optimizer, but are used in a complementary approach.

Section III will show how simple modifications to [3], along with the use of cold S-parameter data, can be used to help overcome the discussed difficulties in determining R_d, $C_{\rm pg}$, and $C_{\rm pd}$.

The one aspect of multibias parameter extraction algorithms that has not been dealt with before is the influence of the bias points used in the extraction on the accuracy and the size of the network that can be extracted. In Section IV, an intelligent bias point selection algorithm is discussed that maximizes the information available to the extraction procedure. The aim of the selection algorithm is to find a relatively small number of bias points from which a consistent model representation can be extracted. Once accurate values for the extrinsic elements are known, they can be de-embedded from the complete set of multibias S-parameters and a nonlinear model can be constructed as was done in [9]. The paper is concluded with a presentation and discussion of experimental results illustrating the accuracy and robustness of the enhanced multibias extraction algorithm.

The goal of the work described here is to develop a modeling procedure that is capable of extracting all the elements of a small-signal model for the construction of bias-dependent small-signal models and nonlinear models of commercial devices, as well as devices under development, using only measured data. This means that no process-related information, such as electromagnetic simulations of the device layout, is allowed as part of the modeling procedure. The reason for this restriction is due to the fact that process-related information is rarely available to users of commercial devices. The requirement of accurately extracting all of the small-signal model elements also places a limit on the complexity of the equivalent circuit models that are used in the modeling procedure. For the results presented in the subsequent sections, the widely published 15-element model topology in Fig. 1 is used.

II. Hybrid Analytical/Decomposition-Based Optimizer

Experience has shown that certain extraction problems are more difficult to solve reliably than others, regardless of the fact that the same type of device with similar dimensions is being modeled. Systematic measurement errors and the fact that the small-signal model is an imperfect approximation of the real device creates a variety of extraction difficulties. This ranges from extraction problems that differ in their sensitivity to the initial optimization values to model elements that consistently converge to nonphysical values. When dealing with measured data, the modeling algorithm therefore needs to be as robust as possible.

Several methods that employ analytical equations as part of an optimization-based extraction approach have been published [4], [5], [8]. In these formulations, the extrinsic elements are optimized, while the intrinsic elements are calculated as a function of the extrinsic elements using analytical equations. The primary advantage of this approach is that it limits the dimensions of the optimization problem to be solved. The formulation in [4] is of special relevance since the procedure is expanded to multibias problems and the analytical equations used are more robust than the more traditional equations found in [10].

The danger of using analytical equations to calculate the intrinsic elements is that the equations may fail in certain instances due to the measured data used and the ill-conditioned nature of the problem. The new hybrid procedure proposed here therefore always uses both optimization and analytical calculations to determine the intrinsic parameters. The two possible solutions for the intrinsic elements are then compared on an element-by-element basis and in each instance the model element providing the best solution is retained.

The following steps describe the operation of the hybrid algorithm.

1) Load the measured data and the optimization initial values and perform the required sensitivity calculations for the decomposition-based optimizer as outlined in [2], [3].
2) Perform one optimization cycle of the subfunctions of the decomposition optimizer as described in [3].

3) Perform the hybrid calculations.

   a) De-embed the current values of the extrinsic elements from the measured data.

   b) Calculate an alternative set of intrinsic elements for each bias point in the extraction using the analytical equations in [4].

   c) Compare each of the optimization-derived intrinsic elements with its corresponding calculated value and choose the element value that provides the lowest modeling error in the elements' associated optimization subfunction. These subfunctions are the same error functions that are used by the decomposition-based optimizer when determining the model element values in step 2).

4) Check if the search termination criteria are satisfied.
5) If no, then go to 2)
6) If yes, then stop.

The above description illustrates how the analytical step is incorporated into the existing optimizer. If step 3) is disabled, the algorithm reverts to the normal decomposition-based optimizer. By using the suboptimization error functions in step 3c), it becomes possible to compare the two solutions on an element-by-element basis. This would not be possible if a global error representing the modeling accuracy of all four S-parameters of a corresponding bias point was used. The global error would be mostly influenced by the dominant model parameters, creating the situation where possible good solutions for the less dominant elements are discarded.

In addition to making the extraction more robust, the hybrid procedure shown above also increases the speed of convergence, especially during the first few iterations when the overall modeling error is large.

III. Data-Driven Extensions to the Multibias Extraction Algorithm

Much attention has been paid in the literature to the difficulties involved in extracting the parasitic gate resistance R_g. R_g is one of the least dominant elements in the model and is highly correlated with the intrinsic channel resistance R_i. The ability to separate the values of these two elements has been one of the motivations behind the development of multibias extraction algorithms.

However, less attention has been paid to the extraction of the parasitic drain resistance R_d. Experience has shown R_d to be the element that least conforms to the assumption of bias independence for the extrinsic elements when extracted from hot S-parameters. For a variety of HEMTs that have been tested, it was found that R_d can assume either very large or very small nonphysical values, while for MESFETs R_d can tend toward negative values. In the case of MESFETs, the behavior of R_d could possibly be linked to high field effects between the gate and drain terminals [11], but for HEMTs no satisfactory physical explanation is known. Unlike R_g, which has very little influence on the overall extraction accuracy, the value of R_d is more critical for the successful determination of the other nondominant elements in the multibias extraction.

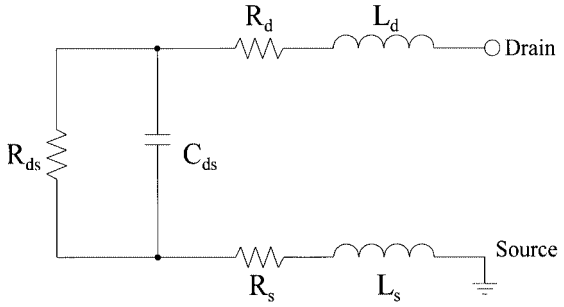

Fig. 2. Simplified representation of the output impedance of a GaAs FET.

In [12], an extraction procedure for determining R_d and R_s using cold bias points with the gate held at a suitably large forward bias was used. Fig. 2 and the equation

$$\begin{aligned}\mathrm{Re}[Z_{\mathrm{out}}] &= \frac{R_{\mathrm{ds}}}{1+\omega^2 C_{\mathrm{ds}}^2 R_{\mathrm{ds}}^2} + R_d + R_s \\ &= \frac{\frac{1}{R_{\mathrm{ds}}}}{\frac{1}{R_{\mathrm{ds}}^2}+\omega^2 C_{\mathrm{ds}}^2} + R_d + R_s \end{aligned} \tag{1}$$

show a simplified representation of the output impedance of a GaAs FET. When V_{GS} is increased, R_{ds} decreases, resulting in the real part of the FET output impedance being dominated by R_d and R_s. It is this behavior that is exploited in [12]. A careful study of (1) shows that a similar result is obtained when R_{ds} assumes very large values, as would be the case when V_{GS} is equal to or less than the pinch-off voltage V_T. Equation (1) also shows that the dominance of R_d and R_s on the output impedance can be further enhanced by using measured data from the upper measurement frequencies. It should be noted that the effect of the parasitic drain capacitance C_{pd} is ignored in Fig. 2 and (1). Unlike direct extraction algorithms, optimizer-based procedures do not need to achieve a near exact separation between the model elements. For a successful extraction, it is only required to find the conditions for which the influence of an element will be more dominant.

A further advantage of using data from cold bias points with $V_{\mathrm{GS}} \leq V_T$ is that the intrinsic model reduces to the three intrinsic capacitor values C_{gs}, C_{gd}, and C_{ds}. The bias points therefore add a minimum of extra parameters to the multibias extraction problem, while providing valuable additional information for determining the solution.

The extraction algorithm in [3] is extended by allowing the user to lock a small-signal model element to a specified list of bias points. Only this subset of the data will be used for the determination of the particular model element. The user also has the possibility to specify the frequency range of the measured data that is to be used in the determination of an element. To determine R_d, the user thus specifies a number of cold bias points with $V_{\mathrm{GS}} \leq V_T$ along with the normally used nonreciprocal data from active bias points. R_d is locked to the cold bias points and no other data is used in the determination of the element. To further aid in the determination of R_d, only measurements made at frequencies above 15 GHz are used.

The second problem experienced in the extraction of the model in Fig. 1 is the separation of the parasitic capacitors C_{pg}

and $C_{\rm pd}$ from the intrinsic capacitors. The parasitic capacitors are separated from the intrinsic capacitors by small series impedances and their values are small when compared to those of the intrinsic capacitors at most bias points. Their values are therefore easily absorbed into the values of the intrinsic capacitors due to the inability of the extraction algorithm to clearly distinguish their effect from the other model elements.

In order to determine $C_{\rm pg}$ and $C_{\rm pd}$, the same extensions as were used for determining R_d can be employed. The parasitic capacitors are locked to the cold S-parameter data with $V_{\rm GS} \leq V_T$ since the intrinsic capacitors generally assume their smallest values in this bias range. The extrinsic capacitors are therefore not as overshadowed as before by the size of the intrinsic capacitors. To further decrease any interaction between the different extrinsic elements, $C_{\rm pg}$ and $C_{\rm pd}$ are only determined from data measured at frequencies below 10 GHz, while the extrinsic inductors and resistors are determined from data measured at frequencies above 15 GHz.

IV. Measurement-Based Active Bias Point Selection Algorithm

The previous section illustrates how cold measurements, along with suitable modifications to the extraction algorithm, can be used to enhance the ability to determine extrinsic elements that are otherwise difficult to extract. The majority of the measured data is, however, still obtained from active bias points where the device is acting as a nonreciprocal two-port. For the extractions presented in [3], the active bias points were selected by hand. A region denoted by a square is picked by the user in the saturated region of the device $I_{\rm DS}$-$V_{\rm DS}$ plane. Bias points at the corners and the center of this square are chosen. Should more bias points be required, they are picked from within the square so as to provide a uniform distribution.

This procedure is in essence driven by the dc curves of the device since the selection tries to uniformly cover the saturated region of the bias plane. The characteristics of the S-parameter data used in the extraction are therefore not considered in the selection of the bias points. The algorithm described in this section overcomes this deficiency by evaluating the S-parameters when choosing suitable bias points.

The algorithm can be divided into two distinct sections. The first section of the algorithm selects a region of the $I_{\rm DS}$–$V_{\rm DS}$ plane in which it is expected that the small-signal model used will be able to accurately approximate the corresponding S-parameter data and the intrinsic elements of the model have well defined values. This subset of the complete multibias data set will in subsequent sections be referred to as the *region of reproducibility*. The second part of the algorithm chooses a subset of bias points from this region so that the S-parameters at the different bias points differ as much as possible from each other. The algorithm therefore tries to maximize the diversity of the measured data that is to be used in the extraction. The driving force behind this selection criterion is the following.

> By maximizing the diversity in the measured data used in the extraction, more emphasis is placed on the elements which are common to the S-parameters from different bias points, namely the effect of the bias-independent extrinsic elements. This aids in the consistent determination of their values, which in turn improves the accuracy with which all the other elements can be determined.

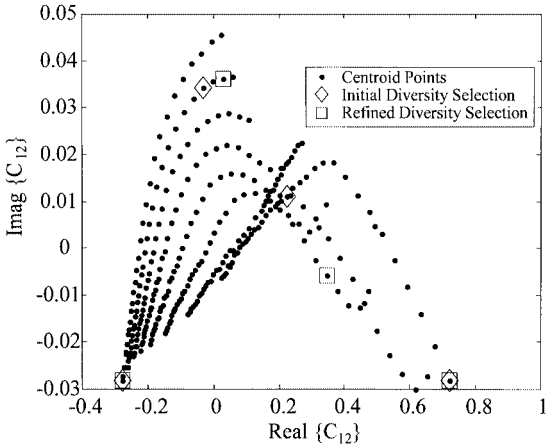

Fig. 3. Scatter plot of the centroids of the S_{12} S-parameters of a pHEMT device. Every • marker represents a centroid C_{12} of an S_{12} S-parameter curve at a different bias point. Changes in the position, orientation, and length of the S_{12} curves due to changes in the bias point of the device is reflected in the change of the C_{12} centroid's position. The centroids marked with ◇ markers represent bias points that were selected with the first algorithm described in Section IV-B. This algorithm performs an initial selection of centroids that are as widely distributed from each other as possible. In the legend this is referred to as the *Initial Diversity Selection*. Centroids marked with □ markers represent changes made in the initial selection (◇ markers) by the second algorithm described in Section IV-B, which attempts to refine the initial selection by improving the distribution of the selected points. Instances where the ◇ and □ markers overlap indicate centroids whose selection were not altered by the refinement procedure.

Each bias point is represented by four different S-parameters, of which each can be viewed as a curve in a complex plane. Each of these curves can change in position, orientation, and length as the bias voltages of the device are changed. In order to implement the above-mentioned algorithms, a simple geometric description of each S-parameter curve is needed that will hide the complexity of each curve, yet make it possible to detect changes in the curve due to changes in the device bias point. The geometric description should not be sensitive to noise in the measured data and be simple to calculate. One such geometric description is the centroid of a curve. The centroid is the mean of the points in the complex plane that make up the S-parameter curve. Each S-parameter is now represented by one complex number and any changes in the length, orientation, or position of the curve is reflected by a change of the centroid's position. In theory, there is an infinite number of curves with different orientations and lengths which will all have the same centroid. However, for the situation considered here, this is unlikely to occur and it is therefore not a practical concern. Fig. 3 illustrates the concept by showing the centroids of the S_{12} S-parameter of a pseudomorphic high electron-mobility transistor (pHEMT) device. Every • marker in Fig. 3 represents a centroid of an S_{12} S-parameter curve at a different bias point.

A. Selecting the Region of Reproducibility From the $I_{\rm DS}$–$V_{\rm DS}$ Plane

As stated before, the *region of reproducibility* is defined as an area of the $I_{\rm DS}$–$V_{\rm DS}$ bias plane where it is expected that

the small-signal model used will be able to accurately approximate the measured S-parameters. In this region of the bias plane, it is also expected that the intrinsic model elements will have well-defined values, which implies that they can be extracted with acceptable accuracy. It is unreasonable to expect that the equivalent circuit small-signal model can provide the same quality of data approximation across the whole range of measured bias points. This observation is substantiated by a range of related experimental evidence [13], [14]. The multibias extraction procedure searches for a solution that simultaneously minimizes the least squares modeling error for a wide range of bias points by using a relatively small number of bias points from the total selection of available data. This solution can then be expanded to the rest of the data by deembedding the extrinsic elements and using analytical equations to determine the values of the intrinsic elements. It is therefore crucial that potential bias points that will negatively impact on the initial multibias extraction be excluded from the selection.

The selection criteria for the region of reproducibility are the following.

- The device must be suitably nonreciprocal at each of the bias points. This ensures that every S-parameter data set used in the multibias extraction provides the maximum amount of additional information for the extraction algorithm. In order to determine if a device is suitably nonreciprocal, a reciprocity factor R is calculated using the centroids for S_{21} and S_{12}. R is defined as

$$R = |C_{21} - C_{12}| \tag{2}$$

where

R reciprocity factor at a specific bias point;
C_{21} centroid of S_{21} at the corresponding bias point;
C_{12} centroid of S_{12} at the corresponding bias point.

The reciprocity factor R is the magnitude of the vector difference between the two complex centroid points and will become zero as the device becomes reciprocal at $V_{\rm DS} = 0$ or when $V_{\rm GS}$ decreases to the point where the device enters its cut-off region. The first step in the algorithm is to determine the bias point at which R has its maximum value. All bias points for which R is less than 20% of $R_{\rm MAX}$ are discarded. This limits the minimum value of $V_{\rm GS}$ that will be used to define the safe region.

- The linear region of the $I_{\rm DS}$–$V_{\rm DS}$ plane is excluded from the allowed selection area. This region is characterized by low $R_{\rm ds}$ element values, making the determination of the intrinsic elements difficult. The S_{22} data for these bias points also show large inductive impedances, leading to the overestimation of the parasitic inductors L_d and L_s. It is this inductive behavior of S_{22} that is used to isolate bias points in or very close to the linear region of the $I_{\rm DS}$–$V_{\rm DS}$ plane. All bias points for which the S_{22} curve has any impedance points in the inductive region of the Smith chart are excluded from the safe selection region. This selection criterion places a limit on the minimum $V_{\rm DS}$ values of the safe region.
- Bias points for which $V_{\rm GS}$ is larger than $V_{\rm GS(max)}$ is excluded from the safe region. $V_{\rm GS(max)}$ is determined from the bias point for which $g_{\rm mDC}$ is a maximum. The intrinsic FET model in Fig. 1 does not contain a resistor $R_{\rm gd}$ in series with $C_{\rm gd}$. A study of the measured intrinsic Y_{12} of a number of HEMT devices indicates that the influence of $R_{\rm gd}$ becomes more pronounced for high $V_{\rm GS}$ voltages and in the linear region. These observations also hold for alternative intrinsic FET models [15] since the assumptions on which they are based are not strictly valid at high $V_{\rm GS}$ voltages. $V_{\rm GS(max)}$ is therefore taken as a convenient and conservative limit to exclude these areas.

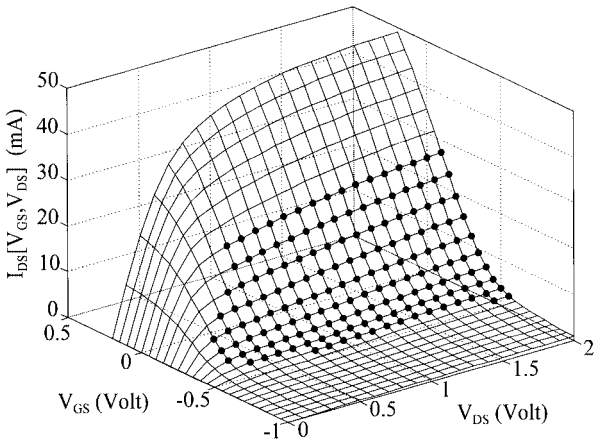

Fig. 4. 3-D representation of $I_{\rm DS}$ as a function of $V_{\rm GS}$ and $V_{\rm DS}$. The bias points shown with a marker are the result of the region of reproducibility selection procedure.

It is important to note that the described linear region identification step employing the phase of S_{22} is only directly applicable to on-wafer and chip devices, since for packaged transistors the reactive influence of the packaging causes additional phase shifts in the S_{11} and S_{22} of the device. Further more, if measured to a high enough frequency, the S_{22} of any device will eventually become inductive. Since the gain of the device decreases with frequency, this can be guarded against in the identification algorithm by monitoring S_{21}.

Of the three selection criteria, the last is the least critical. Depending on the range of bias points over which the device was characterized, it can either be ignored or replaced with a selection criterion that excludes bias points for which the power dissipation $V_{\rm DS} \bullet I_{\rm DS}$ exceeds a user-specified limit. Fig. 4 shows a three-dimensional (3-D) representation of $I_{\rm DS}$ as a function of $V_{\rm GS}$ and $V_{\rm DS}$ for a pHEMT device. The selected bias points are indicated using solid circles. This subset of the measured data is now to be used in the diversity-driven selection algorithm.

B. Diversity-Driven Bias Point Selection Algorithm

The diversity driven selection procedure selects a subset of bias points from the region of reproducibility so that the centroids of the different S-parameters are as far from each other as possible. The selection procedure is applied to each of the four S-parameters separately to ensure that the diversity requirement is satisfied for all the data to be used in the multibias extraction. The results of the four separate selections are then combined to provide a list of distinct bias points for use in the multibias extraction.

The following sequence of steps describes the initial selection algorithm.

1) Initialize the algorithm.

   a) Get the user specified number of points to be selected N_{MAX}.
   b) Normalize the centroid data by removing the mean component from the data and scaling each axis of the two-dimensional (2-D) data set to range from -1 to 1. This set of normalized data is represented by $\mathbf{S}$.
   c) Select the centroid point $\mathbf{c}$ furthest from the mean of the normalized data set $\mathbf{S}$. Point $\mathbf{c}$ represents both the coordinates of the centroid point and the bias voltages V_{GS} and V_{DS} associated with the centroid.
   d) $i = 1, \mathbf{M}^i = \mathbf{c}$. $\mathbf{M}^i$ represents the ith point in the collection $\mathbf{M}$ which is used to store the diversity selected bias points.

2) Evaluate the positions of the data points relative to each other.

   a) Calculate the distance from each point in $\mathbf{S}$ to each of the selected points in $\mathbf{M}$.
   b) Store the minimum calculated distance for each centroid point in $\mathbf{D}$.

3) Select the centroid point $\mathbf{c}$ corresponding with the maximum distance stored in $\mathbf{D}$.
4) $i = i + 1, \mathbf{M}^i = \mathbf{c}$. This represents the next point in the diversity selection.
5) Is $i == N_{\mathrm{MAX}}$?
6) If not, then go to step 2).
7) If yes, then stop.

The normalization of the centroid data as described in step 1b) of the selection algorithm is used to obtain a data set in which the real and imaginary components of the calculated centroids carry equal weight. It should be noted that the normalization procedure used will affect the operation of the selection procedure due to the influence that it has on the distribution of the centroids. Given the fact that there is currently no theoretical basis available for choosing an optimum normalization, the procedure in step 1b) was considered to be the safest alternative.

The scatter plot in Fig. 3 containing the $\mathbf{C_{12}}$ centroid points also shows four points selected with the diversity-driven selection algorithm, indicated with $\diamond$ markers. The bias points selected with the above-described algorithm do not represent the optimum selection of bias points, but they do provide a selection that is close to a local minimum for the problem statement. The first selection can be refined by using a similar algorithm on the already selected points. The refinement step is described by the following sequence of operations.

1) Initialize the algorithm.

   a) Get the selection of bias points $\mathbf{M}$ and the total number of points $\mathbf{S}$ from which the selection was made.
   b) Set the counter $i = 1$.

2) Check if point $\mathbf{M}^i$ should be adjusted to achieve better diversity

   a) Calculate the distance from every point in $\mathbf{S}$ to each selected point $\mathbf{M}^j$, where $j \neq i$.
   b) Store the minimum calculated distance for each point in $\mathbf{S}$ in $\mathbf{D}$.
   c) Replace $\mathbf{M}^i$ with the bias point corresponding to the maximum distance stored in $\mathbf{D}$.

3) $i = i + 1$.
4) Does $i >$ the number of points in $\mathbf{M}$?
5) If no, then go to step 2)
6) Did the content of selection $\mathbf{M}$ change?
7) If yes, then go to step 1b)
8) If no, then stop

The refinement algorithm is very similar to the initial selection procedure, but does not try to add more points to $\mathbf{M}$. It only makes adjustments to the positions of the known points to achieve a selection that provides a local optimum to the distribution problem. In Fig. 3, the result of the refinement step is shown with $\square$ markers. The initial selection used in the refinement are the points indicated with the $\diamond$ markers.

The application of the selection and refinement algorithms described above to each of the four sets of centroids $\mathbf{C_{11}}, \mathbf{C_{21}}, \mathbf{C_{12}}$, and $\mathbf{C_{22}}$ leads to four separate groups that now have to be combined into one unified group. The groups may overlap because the same bias point may satisfy the diversity selection criteria of more than one S-parameter. This problem is solved by removing any duplicate bias points from the selection. A second situation is that different selection groups may have bias points which are distinct, but whose centroid points differ by very little. These bias points can therefore be represented by one bias point. This decreases the number of points in the selection without seriously decreasing the diversity of the S-parameter data.

While the removal of bias points that have been duplicated by the selection procedure is a trivial matter, the trimming of bias points that provide nearly the same information is less so. When the selected bias points are plotted on the I_{DS}–V_{DS} plane of the device (see Fig. 5), one might be tempted to remove selected points that are directly adjacent to each other. This might be in error since it does not take the S-parameter characteristics of the device into account. The following trimming procedure was devised to remove a required number of points from a selection so as to provide the least disturbance to the diversity of the S-parameter data.

1) Initialize algorithm by getting the user specified number of data points r to be trimmed from the selection.
2) Combine the selections $\mathbf{M_{11}}, \mathbf{M_{21}}, \mathbf{M_{12}}$, and $\mathbf{M_{22}}$ into one selection $\mathbf{M}$.
3) Remove any duplicate points in $\mathbf{M}$.
4) $i = 1$.
5) Substitute $\mathbf{M}^i$ with each point in $\mathbf{M}$ that does not come from the same original subselection problem ($\mathbf{M_{11}}, \mathbf{M_{21}}, \mathbf{M_{12}}$, or $\mathbf{M_{22}}$) as $\mathbf{M}^i$, and calculate the distance of the shift in the centroid coordinates caused by each substitution.

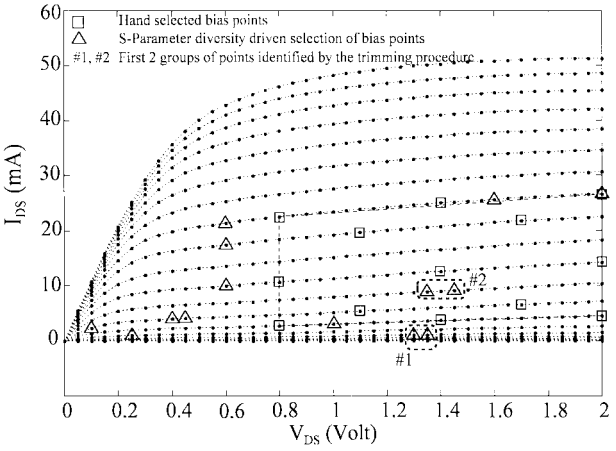

Fig. 5. I_{DS}–V_{DS} curves of a GaAs pHEMT with the bias points selected by various procedures. The bias points indicated by □ markers were selected by hand, while the points indicated with Δ markers were determined with the diversity driven selection procedures. Two sets of bias points as identified by the trimming algorithm are also marked. In each case, these two bias points can be represented by one bias point without seriously decreasing the diversity of the S-parameter data.

6) Store the bias point which causes the minimum shift in the centroid of point $\mathbf{M}^i$ in $\mathbf{A}^i$. This is the associated bias point to $\mathbf{M}^i$.
7) $i = i + 1$.
8) if $i <$ the total number of points in $\mathbf{M}$, then go to step 5).
9) Remove the r bias points from $\mathbf{M}$ which are closest to their associated bias points in $\mathbf{A}$.
10) Stop.

In Fig. 5, the two sets of two points which are the closest to each other in terms of their associated S-parameter data are shown in dashed lines. Note that for the second selection the bias points are not immediately adjacent to each other. In fact, the one remaining instance in which bias points are adjacent to each other provides relatively distinct S-parameter data, highlighting the danger of making decisions purely on the I_{DS}–V_{DS} characteristics of the device.

V. Extraction Results

The effect of the algorithm extensions is illustrated by performing robustness tests on a lattice matched GaAs pHEMT device with a gate length of 0.2 μm and a gate width of 100 μm [16]. Certain examples of this device have been found difficult to model when using the conventional multibias decomposition-based optimizer [3]. The robustness test consists of repeating a particular extraction 20 times while using randomly chosen optimization starting values. The extraction starting values are chosen over a large range using a uniform distribution.

Table I represents a summary of the extrinsic elements obtained with and without the hybrid search options described in Section II. The table provides the range for each element in which the optimization starting values were chosen, as well as the best value, the mean, and the variation Δ of the extracted extrinsic element values. The best value is defined as the parameter corresponding to the extraction with the lowest modeling error, while the variation Δ is defined as the difference between the maximum and minimum extracted element value, thus indicating the range of the solutions in absolute terms. Both multibias extraction experiments used 13 bias points selected using the conventional bias point selection procedure. Fig. 5 contains a plot of the I_{DS}–V_{DS} curves of the device. The active bias points used in the extraction are indicated using square markers. In all the experiments shown here, the measured S-parameter data ranged from 1 to 45 GHz.

TABLE I
Comparison of the Extraction in [3] With the New Hybrid Search Algorithm

	Range of Random Starting Values		Experiment #1 Normal Extractions [3]			Experiment #2 Hybrid Search		
Parameter	Min.	Max.	Best	Mean	Δ	Best	Mean	Δ
Lg (pH)	0.0047	235	69.01	69.35	6.52	63.66	69.86	27.18
Ld (pH)	0.0030	150	50.11	68.69	92.14	50.24	48.68	67.01
Ls (pH)	0.0004	20	11.57	13.75	8.43	9.63	11.56	4.11
Rg (Ω)	0.0003	17.5	0.0004	0.68	3.19	0.70	0.33	4.85
Rd (Ω)	0.0006	30	12.37	9.72	12.62	12.20	12.32	3.90
Rs (Ω)	0.0002	10	2.29	2.52	1.28	2.61	2.45	1.53
Cpg (fF)	0.0020	100	26.60	27.95	3.27	20.07	26.97	29.65
Cpd (fF)	0.0020	100	24.19	27.15	14.51	24.14	23.66	27.48

TABLE II
Comparison of the Influence of the Active Bias Point Selection Method on the Hybrid Search With Cold Bias Point Driven Extensions

	Experiment #3 Hand Selected Active Bias Points			Experiment #4 Diversity Driven Selection of Active Bias Points				Results from [5]
Parameter	Best	Mean	Δ	Best	Mean	Δ	Std %	Std %
Lg (pH)	64.80	63.74	2.85	61.66	60.11	4.37	2.30	1.31
Ld (pH)	53.52	60.41	16.27	51.54	52.16	4.34	2.71	1.44
Ls (pH)	10.66	10.81	2.08	10.53	9.15	2.45	7.15	0.98
Rg (Ω)	4.18	5.30	3.62	3.56	3.69	1.78	12.44	28.38
Rd (Ω)	2.52	2.41	1.54	2.73	2.55	1.00	10.14	0.57
Rs (Ω)	2.10	2.86	2.01	1.68	1.85	1.11	16.13	3.64
Cpg (fF)	21.80	22.08	3.03	18.81	17.69	5.03	7.72	15.48
Cpd (fF)	17.97	20.39	5.74	17.43	16.85	2.32	5.24	28.76

Table II provides comparative test results showing the effect of combining cold S-parameter data with the hybrid search as well as the effect of using active bias points selected with the diversity maximizing algorithm described in Section IV. Both experiments in Table II used the same cold S-parameter data (five bias points) with $V_{GS} \leq V_T$ and the associated extensions discussed in Section III. In both cases, the same number of active bias points, namely 13, were used. Fig. 5 shows the distribution of the active bias points selected with the diversity driven selection procedure.

Table I illustrates that it is not sufficient to simply improve the capabilities of the optimization procedure. The hybrid procedure in Table I does provide better modeling errors in many instances, but it is only when the underlying characteristics of the device and the data are exploited that the results of Table II are obtained. The importance of this is that many published algorithms focus exclusively on improving the capabilities of the optimization algorithm used. Both the experiments in Table I

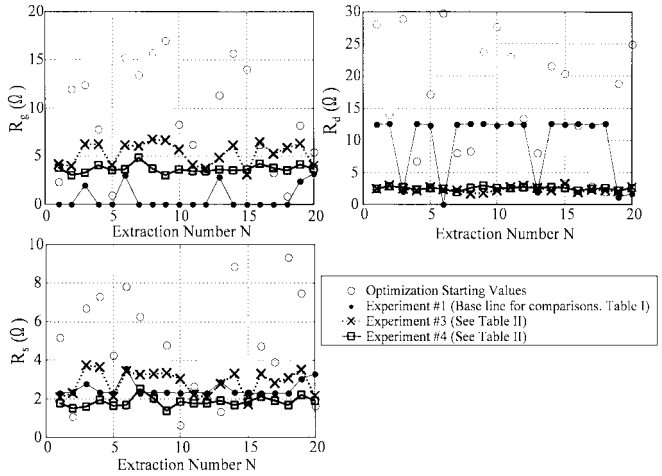

Fig. 6. Comparison of the extracted values of the parasitic extrinsic resistors R_g, R_d, and R_s for three of the experiments presented in Tables I and II. Experiment 1 refers to the first test presented in Table I, while experiments 3 and 4 refer to Table II.

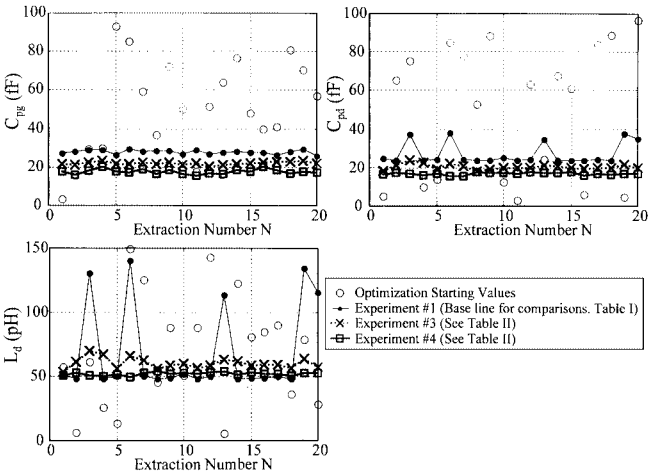

Fig. 7. Comparison of the extracted values of the parasitic extrinsic reactive elements $C_{\rm pg}$, $C_{\rm pd}$, and L_d for three of the experiments presented in Tables I and II. Experiment 1 refers to the first test presented in Table I, while experiments 3 and 4 refer to Table II.

produced elements of whom the majority have values that are physically believable. The exceptions are the parasitic gate and drain resistors R_g and R_d. R_g has a wide range of extracted values, with many tending to the lower optimization boundary. While the variation in R_d is far less, the value of R_d is far larger than what is realistically expected from such an HEMT device. The first experiment in Table II shows that the inclusion of the cold S-parameter data dramatically improves the range of solutions obtained for the extrinsic elements. The mean and best values of the parasitic resistors R_g, R_d, and R_s are closer to each other, but the total variation Δ in their values is still large. This variation Δ decreases considerably with the use of active bias points selected with the diversity-driven selection procedure, as is illustrated by the second experiment in Table II. A comparison of the results in Tables I and II also shows that the various extensions discussed cause a decrease in the difference between the average element values and the best element values for the majority of the extrinsic parameters. The extrinsic elements obtained from the two experiments summarized in Table II are also consistent in their values with each other, despite using different active bias points for the extractions.

A more graphical representation of the test results is given in Figs. 6 and 7. Fig. 6 contains the variation of the three parasitic resistors R_g, R_d, and R_s obtained in three of the robustness tests, namely the first experiment in Table I and the two experiments described in Table II. Fig. 7 provides similar results, but for the parasitic capacitors $C_{\rm pg}$ and $C_{\rm pd}$ and the parasitic inductance L_d. Experience has shown that, of the three parasitic inductors, L_d can be surprisingly difficult to extract. Figs. 6 and 7 clearly indicates how the extensions discussed in this paper help to improve the consistency of the solutions obtained. It also shows the wide range of optimization starting values used in the extractions.

Fig. 8 compares the modeled and the measured S-parameters for the bias point $V_{\rm DS} = 0.6$ V and $I_{\rm DS} = 21.354$ mA. The quality of the fit between the modeled and measured S-parameters seen in Fig. 8 represents the largest modeling errors of all

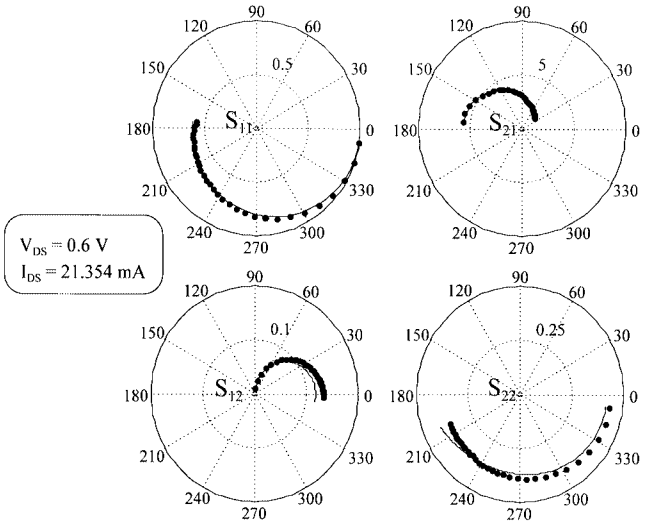

Fig. 8. Comparison of the measured and modeled S-parameters for the bias point that resulted in the largest modeling error. This bias point is close to the knee region of the device $I_{\rm DS}$–$V_{\rm DS}$ curves, which is one of the most difficult areas to model accurately. The measured data is represented by the • markers, while the model generated S-parameters are depicted with the solid line.

the bias points used in the extraction. The indicated bias point is the closest selected point to the knee region of the $I_{\rm DS}$–$V_{\rm DS}$ plane, a difficult area to model. The largest deviations occur in S_{12} and S_{22} and it is suspected that this is due to the omission of $R_{\rm gd}$ in the small-signal model. $R_{\rm ds}$ is also smaller in this region, as is evident from the scale of the S_{22} polar chart. For all the bias points further from the knee region, the modeling deviations in S_{12} and S_{22} are not present and an excellent fit is achieved between the modeled and measured data. What is also clear from Fig. 8 is that the quality of the measured data is high, with no visible signs of resonances or other measurement deviations that can be used to explain the extraction difficulties experienced with this particular device.

The work in [4] and [5] contain the only comparable experimental results for HEMT devices of which we are aware. In both

cases, results are presented for optimization-orientated multibias extraction algorithms that have been subjected to a large number of randomly chosen starting values. Lin and Kompa [4] performed multibias extractions on a chip device that was wire bonded into a test fixture. This leads to far larger extrinsic inductors than those obtained from on-wafer measurements. The larger extrinsic reactive elements greatly help with the separation of the different elements, a fact that was confirmed with simulated measurements generated using the published model parameters [17].

Ghazinour and Jansen [5] presented results from on-wafer measured S-parameters extracted with a hybrid evolutionary/gradient optimization algorithm. Unfortunately, the data in [5] do not make it possible to perform a complete comparison. Ghazinour and Jansen [5] summarize the obtained results by providing the average and the standard deviation of the extracted elements but presents no further information regarding the distribution of the extracted elements. The best individual returned by the evolutionary search, namely the set of model elements providing lowest modeling error, is also not listed. The danger of only using the average and standard deviation in the presentation of the data is that the distribution of the extracted elements is in many instances not Gaussian [2], [17]. When a search fails to find an element, that element in many cases will tend to one of the optimization boundaries. The average value of the element will not always reflect this. Neither will the standard deviation do so if, as in most cases, one of the optimization boundaries are favored. An example of this behavior can be seen for the element R_g in the first experiment in Table I and by looking at the graphical plot of the extracted R_g values in Fig. 6. In the discussion of the results in [5], it is also stated that the values of the parasitic resistors R_g and R_d are very low compared to what is expected from physical considerations.

In order to provide comparative results with [5], the last experiment in Table II was repeated 100 times using random starting values. The standard deviation of the elements was calculated and is expressed as a percentage of the average values obtained. The values found in [5] are also listed. The comparison shows that, with the exception of L_s, the new procedure provides similar or smaller standard deviations for the reactive extrinsic elements. The average value reported for L_s in [5] is 18.30 pH, which is considerably larger than the value listed in Table II. Such a large source inductance will have a far more dominant effect on the system, greatly influencing its extraction accuracy. The parasitic resistors R_d and R_s have larger standard deviations than those reported in [5], but their values correspond to what is expected from physical considerations and the solutions are centred around the average element values.

VI. Conclusion

An improved multibias extraction procedure for GaAs FETs has been presented. The experimental results show that the algorithm is starting value-independent and that it consistently converges to a very small range of solutions for all the model elements. The procedure exploits both the power of a new hybrid search algorithm and the underlying characteristic of the device and the measured S-parameter data to achieve this.

The hybrid optimizer that was discussed favors neither the analytical nor the optimization algorithm. Instead it uses both, accepting the solution that provides the best modeling results. The new analytical calculations are easily integrated into the existing multibias search and add very little computational overhead to the search.

The parameter extraction algorithm also exploits the underlying characteristics of both the device and the measured S-parameter data to further increase its accuracy. While the use of cold bias points to achieve this goal has certain elements in common with direct extraction algorithms, the presented diversity selection algorithm takes the exploitation of the S-parameter characteristics to a new level. The algorithms discussed are made possible by using a simple geometric abstraction for the S-parameter curves. Further uses for these simple geometric representations of S-parameter data are currently being investigated.

A full 15-element small-signal model was extracted from measured S-parameter data using a wide range of randomly chosen optimization starting values. The accuracy of the procedure is such that there is less than a 0.2-Ω difference between the average and the best solution of the extracted values of nondominant elements such as R_g, R_d, and R_s. For the reactive extrinsic elements, the difference between the average and best element values are less than 1.5 nH for the parasitic inductors and less than 1.4 fF for the extrinsic capacitors. This indicates a very high consistency in the solutions obtained by the extraction procedure.

For the development of table-based nonlinear models, S-parameters are measured at anything between 500 and 1300 bias points using an automated measurement system [18]. The parameter extraction approach that has been presented in this paper has attained the required level of robustness that allows it to efficiently process such large data sets. It forms an integral part of algorithms used in the generation of nonlinear models for the purposes of design and technology evaluation [9].

References

[1] G. Dambrine, A. Cappy, F. Heliodore, and E. Playez, "A new method for determining the FET small-signal equivalent circuit," *IEEE Trans. Microwave Theory Tech.*, vol. 36, pp. 1151–1159, July 1988.

[2] C. van Niekerk and P. Meyer, "Performance and limitations of decomposition-based parameter-extraction procedures for FET small-signal models," *IEEE Trans. Microwave Theory Tech.*, vol. 46, pp. 1620–1627, Nov. 1998.

[3] C. van Niekerk, P. Meyer, D. Schreurs, and P. Winson, "A robust integrated multi-bias parameter extraction method for MESFET and HEMT models," *IEEE Trans. Microwave Theory Tech.*, vol. 48, pp. 777–786, May 2000.

[4] F. Lin and G. Kompa, "FET model parameter extraction based on optimization with multiplane data-fitting and bidirectional search—A new concept," *IEEE Trans. Microwave Theory Tech.*, vol. 42, pp. 1114–1121, July 1994.

[5] A. Ghazinour and R. H. Jansen, "Robust, model-independant generation of intrinsic characteristics and multi-bias parameter extraction for MESFETs/HEMTs," in *IEEE MTT-S Int. Microwave Symp. Dig.*, 1998, pp. 149–152.

[6] A. Eskandarian and S. Weinreb, "A note on experimental determination of small-signal equivalent circuit of millimeter-wave FETs," *IEEE Trans. Microwave Theory Tech.*, vol. 41, pp. 159–162, Jan. 1993.

[7] R. Anholt and S. Swirhum, "Equivalent-circuit parameter extraction for cold GaAs MESFET's," *IEEE Trans. Microwave Theory Tech.*, vol. 38, pp. 1243–1247, July 1991.
[8] K. Shirakawa, H. Oikawa, T. Shimura, Y. Kawasaki, Y. Ohashi, T. Saito, and Y. Daido, "An approach to determining an equivalent circuit for HEMT's," *IEEE Trans. Microwave Theory Tech.*, vol. 43, pp. 499–503, Mar. 1995.
[9] D. Schreurs, C. van Niekerk, R. Vandersmissen, and G. Borghs, "Development of extraction and optimization based large-signal models for thinned metamorphic HEMT's on germanium," *Int. J. RF Microwave Computer-Aided Eng.*, vol. 12, no. 5, pp. 439–447, Sept. 2002.
[10] M. Berroth and R. Bosch, "Broad-band determination of the FET small-signal equivalent circuit," *IEEE Trans. Microwave Theory Tech.*, vol. 38, pp. 891–895, July 1990.
[11] T. González and D. Pardo, "Monte Carlo determination of the intrinsic small-signal equivalent circuit of MESFET's," *IEEE Trans. Electron Devices*, vol. 42, pp. 605–611, Apr. 1995.
[12] D. Schreurs, Y. Baeyens, B. K. J. C. Nauwelaers, W. De Raedt, M. Van Hove, and M. Van Rossum, "S-Parameter measurement based quasistatic large-signal cold HEMT model for resistive mixer design," *Int. J. Microwave Millimeter-Wave Computer-Aided Eng.*, vol. 6, no. 4, pp. 250–258, 1996.
[13] R. Anholt, *Electrical and Thermal Characterization of MESFET's, HEMT's, and HBTs.* Norwood, MA: Artech House, 1995.
[14] J. Staudinger, E. Y. Lan, R. Vaitkus, R. Lucero, and J. Hallmark, "An examination of data based large signal models for wireless amplifiers," in *IEEE MTT-S Int. Microwave Symp. Dig.*, 1996, pp. 1747–1750.
[15] P. Jansen, D. Schreurs, W. de Raedt, B. Nauwelaers, and M. Van Rossum, "Consistent small-signal and large-signal extraction techniques for heterojunction FET's," *IEEE Trans. Microwave Theory Tech.*, vol. 43, pp. 87–93, Jan. 1995.
[16] Y. Baeyens, T. Skrabka, M. Van Hove, W. De Raedt, B. Nauwelaers, and M. Van Rossum, "Performance of 0.2 μm planar doped pseudomorfic and lattice matched HEMT's on GaAs and InP for millimeterwave applications," in *Proc. 23rd Eur. Solid State Device Research Conf.*, Grenoble, France, Sept. 13–16, 1993, pp. 753–756.
[17] C. van Niekerk, "Multi-bias decomposition-based optimization for the extraction of small-signal GaAs FET models," Ph.D. dissertation, Univ. Stellenbosch, Stellenbosch, South Africa, 1999.
[18] D. Schreurs, "Measurement based modeling of heterojunction field-effect devices for non-linear microwave circuit design," Ph.D. dissertation, Catholic Univ. Leuven, Leuven, Belgium, 1997.

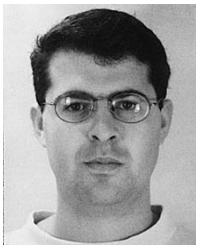

Cornell van Niekerk (S'97–M'99) received the M.Eng. and Ph.D.(Eng.) degrees from the University of Stellenbosch, Stellenbosch, South Africa, in 1996 and 1999, respectively.

In 1998, he joined the staff of the Department of Electrical and Electronic Engineering, University of Stellenbosch, where he is currently a Senior Lecturer. His current research interests are the extraction of transistor CAD models and the use of optimization techniques for the synthesis and refinement of high-frequency designs.

Johan A. du Preez (M'92) was born in South Africa, in 1958. He received the Ph.D. degree in electronic engineering from the University of Stellenbosch, Stellenbosch, South Africa, in 1998. His dissertation focused on efficient high-order hidden Markov modeling.

After an initial four years with the Telecommunications Sector, he joined the Electrical and Electronic Engineering Department, University of Stellenbosch, in mid-1989. Active in the broader fields of signal processing and pattern recognition, his research focuses on biometrics and speech processing.

Dominique M. M.-P. Schreurs (S'90–M'97–SM'02) received the M.Sc. degree in electronic engineering and Ph.D. degree (with honors) from the Katholieke Universiteit Leuven (K.U.Leuven), Leuven, Belgium, in 1992 and 1997, respectively.

She is currently a Post-Doctoral Fellow with the Fund for Scientific Research-Vlaanderen and a Visiting Assistant Professor with the K.U.Leuven. She has been a Visiting Scientist with Agilent Technologies, the Eidgenössische Technische Hochschule (ETH), Zürich, Switzerland, and the National Institute of Standards and Technology (NIST). Her main research interest is the use of vectorial large-signal measurements for the characterization and modeling of nonlinear microwave devices.